Materials Horizons

ROYAL SOCIETY OF CHEMISTRY

COMMUNICATION

View Article Online
View Journal

Cite this: DOI: 10.1039/d3mh00037k

Received 9th January 2023,
Accepted 2nd March 2023

DOI: 10.1039/d3mh00037k

rsc.li/materials-horizons

Switching the memory behaviour from binary to ternary by triggering S_6^{2-} relaxation in polysulfide-bearing zinc–organic complex molecular memories†

Pan-Ke Zhou,‡[a] Xiao-Li Lin,‡[a] Mun Yin Chee,[b] Wen Siang Lew,[b] Tao Zeng,[c] Hao-Hong Li, *[a] Xiong Chen, *[a] Zhi-Rong Chen [a] and Hui-Dong Zheng *[d]

The use of crystalline metal–organic complexes with definite structures as multilevel memories can enable explicit structure–property correlations, which is significant for designing the next generation of memories. Here, four Zn–polysulfide complexes with different degrees of conjugation have been fabricated as memory devices. $ZnS_6(L)_2$-based memories (L = pyridine and 3-methylpyridine) can exhibit only bipolar binary memory performances, but $ZnS_6(L)$-based memories (L = 2,2′-bipyridine and 1,10-phenanthroline) illustrate non-volatile ternary memory performances with high ON2/ON1/OFF ratios ($10^{4.22}/10^{2.27}/1$ and $10^{4.85}/10^{2.58}/1$) and ternary yields (74% and 78%). Their ON1 states stem from the packing adjustments of organic ligands upon the injection of carriers, and the ON2 states are a result of the ring-to-chain relaxation of S_6^{2-} anions. The lower conjugated degrees in $ZnS_6(L)_2$ result in less compact packing; consequently, the adjacent S_6^{2-} rings are too long to trigger the S_6^{2-} relaxation. The deep structure–property correlation in this work provides a new strategy for implementing multilevel memory by triggering polysulfide relaxation based on the conjugated degree regulation of organic ligands.

New concepts

The redox-inactive Zn^{2+} ion in a tetrahedral crystal field was used as a metal center to prepare a series of Zn/polysulfide/organic complexes, *i.e.*, $ZnS_6(Py)_2$ (**1**; Py = pyridine), $ZnS_6(Mpy)_2$ (**2**; Mpy = 3-methylpyridine), $ZnS_6(Bipy)$ (**3**; Bipy = 2,2′-bipyridine), and $ZnS_6(Phen)$ (**4**; Phen = 1,10-phenanthroline), which were further fabricated as memory devices with a sandwiched structure of FTO/Zn-complex/Ag. Interestingly, their memory performance can be elevated from binary to ternary by triggering the ring-to-chain relaxation of S_6^{2-} anions. This work opens up a new route for implementing multilevel memory with low cost.

Introduction

The coming big-data era calls for new non-volatile memories that have larger storage densities, higher computing speeds and low costs.[1] Multilevel memory has been considered as the best candidate for next-generation memory, in which the device can present three or more conductive states, from which, consequently, a revolutionary storage density increase will be achieved.[2–4] A wide range of active components have been fabricated as multilevel resistive memory devices, including organic small molecules,[5–9] polymers and their composites,[2,10–12] inorganic oxide/nitrides[13–15] and biomaterials.[16,17] However, many technical problems still need to be solved. For instance, organic or biomaterial-based devices suffer from insufficient reproducibility/endurance/scalability, diverse threshold voltage distributions, low switching speeds, long-term environmental instability and low ternary yields (about 30–50%).[4,18–20] Inorganic memories require harsh processing conditions with poor defect sensitivity.[21] Importantly, due to the inherent structural complexities of the active components and electrode/organic interfaces, our understanding of the multilevel switching mechanism is still very poor, which renders difficulties with device optimization.[22] So far, the proposed mechanisms, such as field-driven polarization, conformation changes or redox transitions, still lack direct evidence because the coupling of injected carriers with the disordered materials is

[a] Fujian Provincial Key Laboratory of Advanced Inorganic Oxygenated Materials, State Key Laboratory of Photocatalysis on Energy and Environment, College of Chemistry, Fuzhou University, Fujian 350108, China. E-mail: lihh@fzu.edu.cn, chenxiong987@fzu.edu.cn

[b] School of Physical and Mathematical Sciences, Nanyang Technological University, Singapore 637371, Singapore

[c] Department of Materials Science and Engineering, National University of Singapore, Singapore 117575, Singapore

[d] Fujian Engineering Research Centre of Advanced Manufacturing Technology for Fine Chemicals, College of Chemical Engineering, Fuzhou University, Fuzhou, Fujian, 350108, China. E-mail: youngman@fzu.edu.cn

† Electronic supplementary information (ESI) available: experimental section and supplementary figures. CCDC 2232734–2232737. For ESI and crystallographic data in CIF or other electronic format see DOI: https://doi.org/10.1039/d3mh00037k

‡ These authors contributed equally to this work.

very complicated.[23,24] Therefore, the overall commercial translation of these memories remains difficult.[25]

Because of the explicit structure–property relationships and adjustable electrical multi-states, crystalline metal–organic complexes have exhibited fascinating applications in new kinds of memory.[26–28] Their optical/electrical properties can be manipulated *via* the functional modification of organic ligands, resulting in the presence of binary or multilevel conductive states.[29–31] So far, some small-molecule metal–organic complexes have also been applied to resistive memories, including Cr,[32] Fe,[33,34] Co,[35] Ni,[36] Cu,[37] Ru,[38,39] Rh,[40] Ir,[41] Pt,[42,43] Au[44–46] and rare earth-based complexes.[47] However, most of the metal complex-based devices are binary memories, and only a limited number that are based on complicated function modification on organic ligands are ternary.[32,34,44,45] In this system, implementing multilevel memories with lost cost and clarifying their resistive switching mechanisms are challenging.[26] Polysulfides (S_n^{2-}) are important intermediates in many fields, such as lithium-ion batteries and desulfurization processes in fossil fuels.[48] As soft ligands, polysulfides are fascinating and versatile ligands for tuning the structures/properties of new functional materials.[49] Their good flexibility provides a new strategy for the realization of multilevel memory, which has never been investigated in memory devices. Zn(II) is redox-inactive,[50] which can rule out the redox/reduction process under an external voltage. Compared with other transition metals such as Ni(II) or Mg(II), more facile ligand-exchange reactions will occur on the Zn(II) center owing to the almost equal affinity around its coordinated sphere.[51] In this work, the redox-inactive Zn^{2+} ion in a tetrahedral crystal field was used as a metal center to prepare a series of Zn/polysulfide/organic complexes, *i.e.*, $ZnS_6(Py)_2$ (**1**; Py = pyridine), $ZnS_6(Mpy)_2$ (**2**; Mpy = 3-methylpyridine), $ZnS_6(Bipy)$ (**3**; Bipy = 2,2'-bipyridine), and $ZnS_6(Phen)$ (**4**; Phen = 1,10-phenanthroline), which were further fabricated as memory devices with a sandwiched structure of FTO/Zn-complex/Ag. Interestingly, their memory performances can be elevated from binary to ternary by triggering the ring-to-chain relaxation of S_6^{2-} anions. This work opens up a new avenue for implementing multilevel memory with low cost.

Results and discussion

The complexes $ZnS_6(Py)_2$ (**1**), $ZnS_6(Mpy)_2$ (**2**), $ZnS_6(Bipy)$ (**3**) and $ZnS_6(Phen)$ (**4**) have previously been documented.[48,52,53] The Zn centers are all in tetrahedral environments coordinated by two nitrogen atoms of organic ligands and two sulfur atoms of S_6^{2-} ions (Fig. 1). The Zn–N (2.069(2)–2.089(6) Å), Zn–S (2.262(3)–2.3093(14) Å) and S–S (2.019(4)–2.079(2) Å) lengths are in the normal range (Table S1, ESI†). The bond angles around the tetrahedra are 103.06(12)–125.24(5)°, implying their distorted geometries (Table S1, ESI†). The S–S–S bond angles of 106.23(10)–108.75(9)° are consistent with the literature.[54] The dihedral angles between the two pyridine rings in **1** and **2** are 84.433 and 52.016°, respectively, and the bipyridine and 1,10-phenanthroline ligands in **3** and **4**, respectively, are planar.

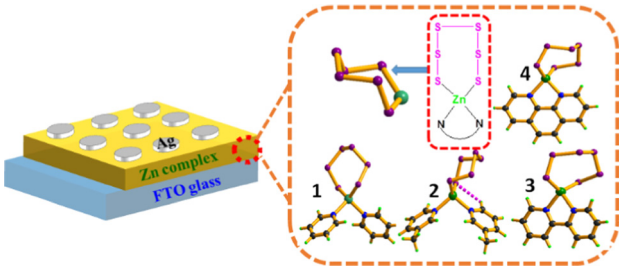

Fig. 1 3D schematic diagram of FTO/Zn complex/Ag devices showing the structure of Zn-complexes containing ZnS_6 in the chair conformation: (**1**) $ZnS_6(Py)_2$, (**2**) $ZnS_6(Mpy)_2$, (**3**) $ZnS_6(Bipy)$ and (**4**) $ZnS_6(Phen)$.

All the S_6^{2-} anions adopt the chair conformation (Fig. 1). No weak interactions can be found in **1**, but the intramolecular C–H···S hydrogen bond in **2** hinders the rotation of the pyridine rings, resulting in a smaller dihedral angle (Table S3, ESI†). The centroid distances between the pyridine rings of **1** and **2** are 3.885(2) and 4.043(3) Å, respectively, implying the absence of π···π stacking interactions. The S_6^{2-} anions are separated by organic ligands (Fig. 2a). In **3** with bipyridine as the ligand, relatively weak π···π stacking interactions among the pyridine rings with centroid distances of 3.715(4) Å can be observed (Table S4, ESI†). Together with inter-molecular C–H···S hydrogen bonds (Table S3, ESI†), a $[ZnS_6(Bipy)]_2$ dimer with the J-aggregation mode is generated (Fig. 2b). A similar structural character can be seen in **4**, whose J-aggregated $[ZnS_6(Phen)]_2$ dimer is constructed from strong π···π stacking interactions among the phenanthroline rings (centroid distances: 3.534(4)–3.650(5) Å) and the C–H···S hydrogen bonds (Fig. 2c). The nearest S···S distances between neighboring dimers in **3** and **4** are 3.4649(7) and 3.6998(4) Å, respectively, hinting at possible S_6^{2-} relaxation upon external stimulus. Finally, the adjacent $[ZnS_6(L)]_2$ (L = Bipy or Phen) dimers are linked into a 1-D chain through strong π···π stacking interactions (Fig. 2d). These complexes were further characterized *via* PXRD, FT-IR, Raman, UV-vis and TGA. The accordance of experimental PXRD patterns with the simulation results verifies the purity of the as-synthesized complexes (Fig. S1, ESI†). In the FT-IR spectra, the characteristic stretching vibrations of C–H

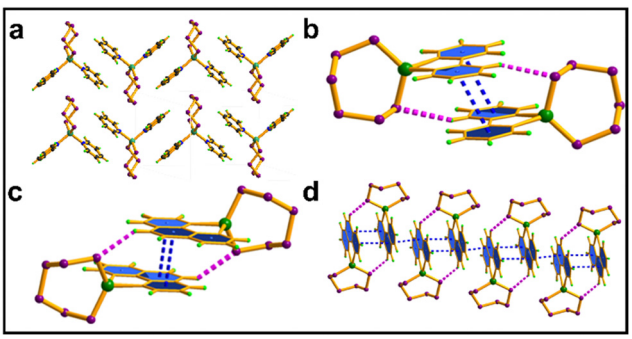

Fig. 2 (a) Packing diagram of $ZnS_6(Py)_2$ showing the positions of S_6^{2-} being separated by ligands. Structures of the dimers with J-aggregation modes for (b) $[ZnS_6(Bipy)]_2$, and (c) $[ZnS_6(Phen)]_2$. (d) 1-D chain based on π···π stacking interactions in $[ZnS_6(Phen)]$.

(3050 cm^{-1}), C=C (1600 cm^{-1}), C=N (1450 cm^{-1}) and S–S (494 cm^{-1}) can be observed (Fig. S2a, ESI†). Meanwhile, in the Raman spectra, the Zn–S/N vibrations appear at around 190 and 300 cm^{-1} (Fig. S2b, ESI†).[55] The UV-vis adsorptions can be attributed to the π–π* transitions in the organic ligands and S_6^{2-} anions (Figure. S2c, ESI†).[48,53] After their dissolution in DMF, the discrete adsorptions indicate the presence of isolated Zn-complexes without any weak interactions, which can return to be continuous on FTO films (Fig. S2d, ESI†). The thermal stabilities, determined from their TGA curves (defined as 5% weight loss), were estimated as 97 °C (**1**), 116 °C (**2**), 230 °C (**3**) and 252 °C (**4**) (Fig. S2e, ESI†). These results demonstrate that the higher degree of conjugation is helpful for improving the thermal stability, which will further ensure device stability due, for example, to inevitable Joule heating during the course of voltage operation.[56]

The 3D schematic diagram of the FTO/Zn-complex/Ag devices is depicted in Fig. 1, which were fabricated using the spin-coating method. The surface morphologies detected using SEM and AFM are shown in Fig. 3, and the cross-sectional images are illustrated in Fig. S3 (ESI†). The surface morphologies monitored *via* SEM illustrate that all the FTO/Zn-complex films are composed of uniform nanosphere particles, whose average diameters are about 253, 300, 320 and 329 nm, respectively, for **1**–**4** (Fig. 3), and their surface roughness was validated using AFM, whose respective root-mean-square (rms) values are 11.30, 12.40, 13.30 and 14.00 nm (Fig. 3). The film thicknesses are in the range of 253.0–719.1 nm, as estimated from the cross-sectional SEM images (Fig. S3, ESI†). In the memories using distinct crystalline phases as active layers, the memory performances are not thickness-dependent.[57] Thus, the thickness effect can be omitted. XRD measurements on the FTO substrate were also carried out, and their good consistency indicates the maintenance of crystalline states, which illustrates typical single-crystalline thin films with the maintenance of crystalline states (Fig. S4, ESI†).

The current–voltage (*I*–*V*) curves recorded in the voltage sweep of 0 V → +5 V → 0 V → −5 V → 0 V under a current compliance of 0.5 A for the four FTO/Zn-complex/Ag devices are shown in Fig. 4a, and their high-resistance state (HRS), middle-resistance state (MRS), low-resistance state (LRS) currents are shown in Fig. 4b. Fig. S5 (ESI†) shows the cumulative probability (CP) of the distribution of the HRS and LRS values for the FTO/Zn-complex/Ag memories, whose coefficient of variation values ($C_v = \sigma/\mu$, where σ is the standard deviation and μ is the mean value) are shown in Fig. 4c and Table S5 (ESI†). The C_v value of the HRS, LRS, V_{th1} and V_{th2} for the device based on **4** are 0.20, 0.17, 0.18 and 0.12, respectively. The above results indicate that the devices show good uniformity and stability. Clearly, the FTO/**1**/Ag and FTO/**2**/Ag devices exhibit typical bipolar binary non-volatile memory performances, but the FTO/**3**/Ag and FTO/**4**/Ag devices illustrate a non-volatile WORM (write-once read-many-times) ternary memory performance. Their important resistive switching parameters are summarized in Table S6 (ESI†). In the *I*–*V* curve of the FTO/**1**/Ag device (Fig. S6a, ESI†), the jump from the HRS (OFF state, $10^{-4.31}$ A) to the LRS (ON state, $10^{-2.27}$ A) can occur at 0.41 V (V_{Set}) in the first scanning range of 0 → +5 V (sweep 1), which can be retained in the second scanning range of +5 V → 0V (sweep 2). In the third sweep from 0 → −5 V (sweep 3), it turns back into the HRS *via* a "Reset" operation at −3.97 V. The device remains in this HRS in the fourth scanning range to complete this loop (sweep 4). The ON/OFF ratio can be calculated as $10^{2.04}$ using 0.1 V as the reading voltage. The resistive switching behaviour is repeatable, which can be validated *via* the stable HRS/LRS currents (Fig. S6b, ESI†) and the good distribution of V_{Set}/V_{Reset} (Fig. S6c, ESI†) in 10 sweep cycles. Its endurance can be further verified by 100 continuous cycles (Fig. S6d, ESI†). Furthermore, the retention time is an important parameter to evaluate the reliability of memory devices. The current states of the FTO/**1**/Ag device show no significant degradation over 3.6 × 10^3 s under a constant voltage of +0.1 V, as shown in Fig. S6e (ESI†).

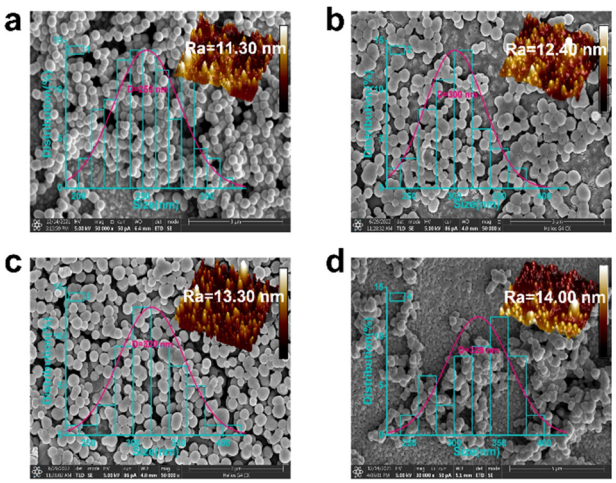

Fig. 3 Surface morphologies of the FTO/Zn-complex films (insets: AFM images of the films): (a) FTO/**1**; (b) FTO/**2**; (c) FTO/**3**; and (d) FTO/**4**.

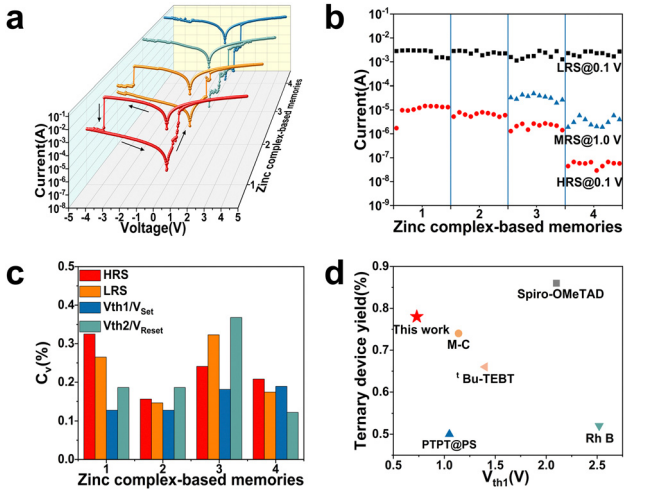

Fig. 4 (a) *I*–*V* curves of the four memory devices; (b) HRS, MRS and LRS states: 1 (FTO/**1**/Ag); 2 (FTO/**2**/Ag); 3 (FTO/**3**/Ag); and 4 (FTO/**4**/Ag); (c) C_v values of the Zn-complex-based devices; and (d) comparison of the V_{th1} and ternary yield of the FTO/**4**/Ag device with reported ternary memories.

The FTO/**2**/Ag device reveals a similar RRAM-resistive switching behaviour with an ON/OFF ratio of $10^{2.02}$, a V_{Set}/V_{Reset} of +0.81/−3.17 V and good endurance (Fig. S7, ESI†).

The non-volatile WORM ternary memory performance of FTO/**3**/Ag can be deduced from its *I*–*V* curve (Fig. S8a, ESI†). In the first sweeping range (0 → +5.0 V, sweep 1), the current jumping from the HRS (OFF state, $10^{-6.16}$ A) to the MRS (ON1 state, $10^{-3.89}$ A) can occur at 0.58 V (V_{th1}), and then a further change to the LRS (ON2 state, $10^{-1.94}$ A) happens at 1.47 V (V_{th2}). The LRS can be maintained in sweeps 2 and 3. The ON2/ON1/OFF current ratio is $10^{4.22}/10^{2.27}/1$, demonstrating a typical ternary memory performance.[2,58] The ternary resistive switching behaviour can be reproduced, which is validated by the uniform HRS, MRS and LRS currents under constant stress voltages of +0.1 and +1.0 V (Fig. S8b, ESI†). The narrow V_{th1} and V_{th2} distributions measured from the ten separate memory cells also imply its good reproducibility (Fig. S8c, ESI†). Moreover, the device stability can be further validated by 100 cycles of testing of the two states (Fig. S8d, ESI†). Its retention stability can be verified by 3.6×10^3 s retention measurement (Fig. S8e, ESI†). The ternary yield can reach 74%, which is considerable compared with other ternary memories.[17] The FTO/**4**/Ag device exhibits similar ternary WORM memory behaviour with a larger ON2/ON1/OFF ratio ($10^{4.85}/10^{2.58}/1$), lower threshold voltages (0.73/1.29 V), good retention stability and a higher ternary yield (78%) (Fig. S9, ESI†). The ON2/ON1/OFF ratio of these WORM ternary devices is comparable to reported devices (ITO/Azo/Al, ITO/OZA-SO/Al), but the set voltages (0.58/1.47 V and +0.73/+1.29 V) are much lower (for example, −1.37/−2.09 V for ITO/Azo/Al) (Table S7, ESI†).[59,60] In particular, the ternary yields of 74% and 78% are much higher than most of the ternary memories (about 30–50%),[5] but are still lower than the current highest value of 86% (Fig. 4d).[61] The better ternary memory performance of the FTO/**4**/Ag device is relative to its larger conjugated system and strong π···π stacking interactions, in which charged defects will be inhibited.

The mechanism of the improvement from binary to ternary memory performance in these FTO/Zn-complex/Ag devices was clarified. Two model devices with the structure of Ag/Zn-complex/Ag were prepared, in which the Ag/**1**/Ag and Ag/**3**/Ag devices were simulated as binary and ternary performances, respectively. Then SEM, together with EDS measurements, were conducted on these model devices before and after the setting operations (Fig. S10, ESI†). After the setting operation, no Ag filaments can be detected between the two Ag electrodes, which rules out the filament penetration mechanism in these devices. Re-plotting of the double logarithm (log–log) on the *I*–*V* curves in positive and negative voltage sweep regions was conducted using Ohmic and space-charge limited conduction (SCLC) models,[62] and their log(*I*)–log(*V*) characteristics are given in Fig. S11 (ESI†). FTO/**1**/Ag and FTO/**3**/Ag are described as examples of binary and ternary processes, respectively. In the negative sweep region of the binary FTO/**1**/Ag device, three different slopes correspond to different conductive states, *i.e.*, an Ohmic region (slope: 1.26, $I \propto V$), an SCLC region (slope: 2.60, $I \propto V^2$) and another Ohmic region (slope: 1.05)

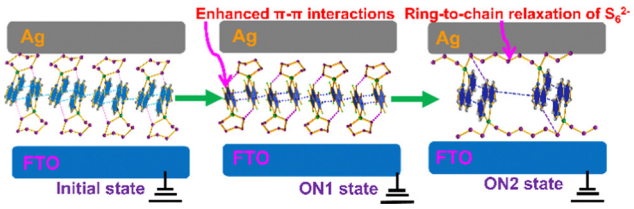

Fig. 5 Proposed binary/ternary resistive switching mechanisms.

(Fig. S11a, ESI†). In the negative sweep region of the ternary FTO/**3**/Ag device, four slopes can be assigned as follows: Ohmic region (0.95), the first SCLC region (3.11), the second SCLC region (4.11) and another Ohmic region (1.18) (Fig. S11e, ESI†). Similar log(*I*)–log(*V*) characteristics can be seen in other devices in their positive sweep region (Fig. S11b and S11d, ESI†). The above information indicates that the binary/ternary resistive switching behaviour in these FTO/Zn-complex/Ag devices stems from the charge trapping/releasing SCLC processes. It has been proved that the S_8 ring can undergo ring-to-chain structural relaxation upon photoexcitation, which might also happen upon the application of an external voltage.[63] Based on the structural characteristics of the four Zn/polysulfide/organic complexes and the above information, the following resistive switching mechanisms were proposed (Fig. 5). The binary memory behaviour of the FTO/**1**/Ag and FTO/**2**/Ag devices stems from the conformational changes of the pyridine/3-methylpyridine ligands upon electrical stimulation, based on which the ON currents can flow along organic ligands with strong π–π interactions. In the ternary memories of the FTO/**3**/Ag and FTO/**4**/Ag devices, the ON1 currents also originate from conduction along the organic ligands upon the injection of carriers, and the ON2 currents are the result of ring-to-chain relaxation of the S_6^{2-} anions into 1-D ZnS_n chains.

The above conjecture can be validated, firstly through Kelvin probe force microscopy (KPFM) measurements, which verify the charge trapping process in the Zn-complex layers. During negative sweeping, the Zn-complex can trap the injected carriers from the electrodes, which can be visualized in the KPFM diagrams (Fig. 6). The bright regions in the surface potential indicate the increased surface potential, which is led by the trapped charges within the Zn-complexes.[64] The potential differences between charge-trapped and non-trapped regions are 22.0 mV (FTO/**1**), 29.3 mV (FTO/**2**), 64.8 mV (FTO/**3**) and 1182.0 mV (FTO/**4**), validating the charge trapping processes and continuous carrier hopping pathway in the Zn-complex layers. Clearly, the FTO/**4** film exhibits a much higher potential difference, suggesting its strong carrier capturing capability. Secondly, in the voltage-dependent XRD patterns of FTO/**2**, after a set operation, the peak at $2\theta = 42.00^\circ$ can be greatly strengthened, and a new diffraction peak at 48.96° appears (Fig. S12a, ESI†). This indicates lattice shifts induced by the formation of π–π interactions among the conformationally changed pyridine/3-methylpyridine ligands. However, in the voltage-dependent XRD patterns of the FTO/**3** film, we could not find any shifts after set processes (Fig. S12b, ESI†) because

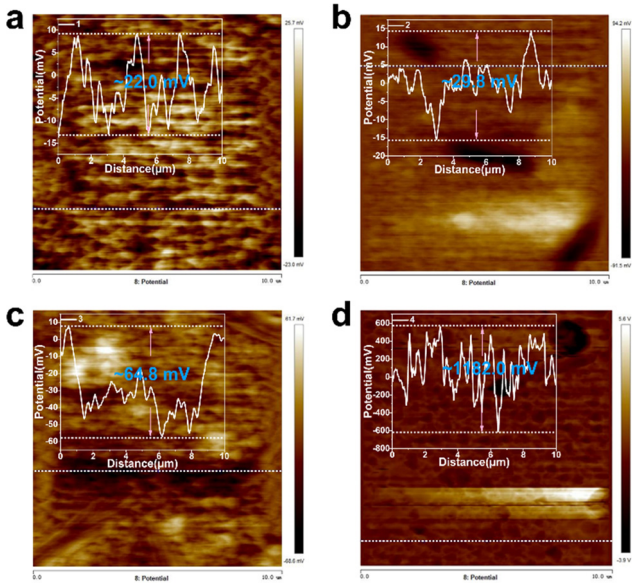

Fig. 6 KPFM surface potential distributions and randomly selected line profiles: (a) FTO/**1**; (b) FTO/**2**; (c) FTO/**3**; and (d) FTO/**4**.

the strong π–π interactions existed in their initial states according to structural analysis (Fig. 2). Thirdly, as indicated in the CV curves, there is only one pair of oxidation/reduction peaks in complexes **1** and **2** (+1.00/−0.84 V for **1**, +1.27/−1.21 V for **2**), which correspond to the oxidation/reduction of Zn^{II}/Zn^{0} (Fig. 7a).[65] However, in the CV curves of complexes **3** and **4**, a new couple of weak peaks can be observed (−0.13/−0.46 V for **3**, +0.01/−0.48 V for **4**), which can be assigned to the oxidation/reduction of S_6^{2-} (Fig. 7b).[65] This information points to the occurrence of S_6^{2-} anion relaxation in the FTO/**3**/Ag and FTO/**4**/Ag devices under an external voltage, which did not happen in the FTO/**1**/Ag and FTO/**2**/Ag devices. Finally, electron spin resonance (ESR) suggests that **1** and **2** are ESR silent, but the presence of paramagnetic signals for **3** and **4** is assigned to cleavage of the S–S bonds in S_6^{2-} anions to generate reactive sulfur radicals (Fig. 7).[66] The reason for the absence of ring-to-chain S_6^{2-} relaxation in the FTO/**1**/Ag and FTO/**2**/Ag devices can be explained as follows: the lower degrees of conjugation for pyridine and 3-methylpyridine result in less compact packing, so the adjacent S_6^{2-} rings are too long to execute ring-to-chain relaxations. Besides, the adjacent S_6^{2-} anions have been separated by the pyridine ligands, which prevent the formation of 1-D ZnS_n chains. The above experimental facts support well the resistive switching mechanisms.

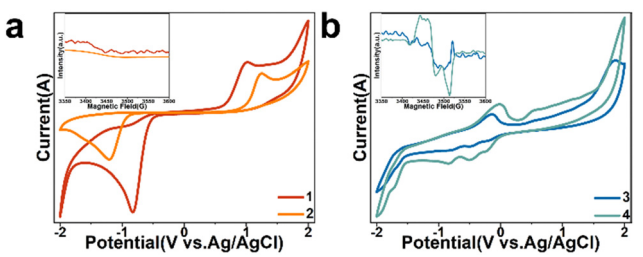

Fig. 7 CV curves of the four complexes (insets: EPR spectra of the four complexes): (a) **1** and **2**; and (b) **3** and **4**.

Conclusions

In summary, $ZnS_6(L)_2$ complexes containing ligands with low conjugation can only exhibit normal binary memory performances, but those bearing ligands with greater conjugation can present ternary memory performances with high ON2/ON1/OFF ratios ($10^{4.22}/10^{2.27}/1$ and $10^{4.85}/10^{2.58}/1$) and ternary yields (74% and 78%). The ON2 state is triggered by the ring-to-chain relaxation of S_6^{2-} anions. When the lower-conjugation ligands are used, less compact packing can be observed, and the adjacent S_6^{2-} rings are too long to trigger the S_6^{2-} relaxations. The deep structure–property correlation together with the use of cheap polysulfide/organic ligands paves the way for implementing new multilevel memories with low costs.

Author contributions

Pan-Ke Zhou: investigation, methodology, formal analysis, writing – original draft. Xiao-Li Lin: investigation, methodology. Mun Yin Chee: data curation. Wen Siang Lew: data curation. Tao Zeng: data curation. Hao-Hong Li: conceptualization, writing – review and editing, supervision, funding acquisition. Xiong Chen: conceptualization, supervision. Zhi-Rong Chen: supervision. Hui-Dong Zheng: supervision, funding acquisition.

Conflicts of interest

There are no conflicts to declare.

Acknowledgements

This work was financially supported by the Key Program of Qingyuan Innovation Laboratory (Grant No. 00221001), the National Natural Science Foundation of China (No. 22078065), the Natural Science Foundation of Fujian Province of China (2021J02007, 2021J01553) and the Fujian Science & Technology Innovation Laboratory for Optoelectronic Information of China (2021ZR148).

References

1 H. S. P. Wong and S. Salahuddin, *Nat. Nanotechnol.*, 2015, **10**, 191–194.
2 P. K. Zhou, L. L. Zong, K. Y. Song, Z. C. Yang, H. H. Li and Z. R. Chen, *ACS Appl. Mater. Interfaces*, 2021, **13**, 50350–50357.
3 Q. j Zhang, H. Li, Q. F. Xu, J. H. He, D. Y. Chen, N. J. Li and J. M. Lu, *J. Mater. Chem. C*, 2019, **7**, 4863–4869.
4 C. Tan, Z. Liu, W. Huang and H. Zhang, *Chem. Soc. Rev.*, 2015, **44**, 2615–2628.
5 Q. Zhang, J. He, H. Zhuang, H. Li, N. Li, Q. Xu, D. Chen and J. M. Lu, *Adv. Funct. Mater.*, 2016, **26**, 146–154.

6 Y. Li, C. Zhang, S. Ling, C. Ma, J. Zhang, Y. Jiang, R. Zhao, H. Li, J. Lu and Q. Zhang, *Small*, 2021, **17**, 2100102.
7 H. Cao, Q. Zhang, H. Li and J. M. Lu, *J. Mater. Chem. C*, 2021, **9**, 569–574.
8 J. Wang, X. F. Cheng, W. H. Qian, Y. Y. Zhao, J. H. He, Q. F. Xu, H. Li, D. Y. Chen, N. J. Li and J. M. Lu, *J. Mater. Chem. C*, 2020, **8**, 7658–7662.
9 C. Zhang, H. Li, Y. Su, F. Yu, C. Li, Q. Zhang and J. M. Lu, *Mater. Chem. Front.*, 2020, **4**, 3280–3289.
10 S. J. Liu, P. Wang, Q. Zhao, H. Y. Yang, J. Wong, H. B. Sun, X. C. Dong, W. P. Lin and W. Huang, *Adv. Mater.*, 2012, **24**, 2901–2905.
11 Z. Lv, Y. Wang, Z. Chen, L. Sun, J. Wang, M. Chen, Z. Xu, Q. Liao, L. Zhou, X. Chen, J. Li, K. Zhou, Y. Zhou, Y. J. Zeng, S. T. Han and V. A. L. Roy, *Adv. Sci.*, 2018, **5**, 1800714.
12 C. Ye, Q. Peng, M. Li, J. Luo, Z. Tang, J. Pei, J. Chen, Z. Shuai, L. Jiang and Y. Song, *J. Am. Chem. Soc.*, 2012, **134**, 20053–20059.
13 W. H. Qian, X. F. Cheng, Y. Y. Zhao, J. Zhou, J. H. He, H. Li, Q. F. Xu, N. J. Li, D. Y. Chen and J. M. Lu, *Adv. Mater.*, 2019, **31**, 1806424.
14 D. E. McCoy, T. Feo, T. A. Harvey and R. O. Prum, *Nat. Commun.*, 2018, **9**, 1.
15 W. J. Sun, Y. Y. Zhao, X. F. Cheng, J. H. He and J. M. Lu, *ACS Appl. Mater. Interfaces*, 2020, **12**, 9865–9871.
16 H. Wang, F. Meng, Y. Cai, L. Zheng, Y. Li, Y. Liu, Y. Jiang, X. Wang and X. Chen, *Adv. Mater.*, 2013, **25**, 5498–5503.
17 R. J. Tseng, C. Tsai, L. Ma, J. Ouyang, C. S. Ozkan and Y. Yang, *Nat. Nanotechnol.*, 2006, **1**, 72–77.
18 Z. Liu, J. He, H. Li, Q. Xu, N. Li, D. Chen, L. Wang, X. Chen, K. Zhang and J. Lu, *Adv. Electron. Mater.*, 2016, **2**, 1500474.
19 E. Shi, J. He, H. Zhuang, H. Liu, Y. Zheng, H. Li, Q. Xu, J. Zheng and J. Lu, *J. Mater. Chem. C*, 2016, **4**, 2579–2586.
20 W. P. Lin, S. J. Liu, T. Gong, Q. Zhao and W. Huang, *Adv. Mater.*, 2014, **26**, 570–606.
21 P. Yang, Y. J. Noh, Y.-J. Baek, H. Zheng, C. J. Kang, H. H. Lee and T. S. Yoon, *Appl. Phys. Lett.*, 2016, **108**, 052108.
22 Y. Yang, P. Gao, S. Gaba, T. Chang, X. Pan and W. Lu, *Nat. Commun.*, 2012, **3**, 732.
23 A. Bandyopadhyay, S. Sahu and M. Higuchi, *J. Am. Chem. Soc.*, 2011, **133**, 1168–1171.
24 P. Y. Gu, F. Zhou, J. Gao, G. Li, C. Wang, Q. F. Xu, Q. Zhang and J. M. Lu, *J. Am. Chem. Soc.*, 2013, **135**, 14086–14089.
25 D. Xiang, X. Wang, C. Jia, T. Lee and X. Guo, *Chem. Rev.*, 2016, **116**, 4318–4440.
26 Y. Wang, D. Astruc and A. S. Abd-El-Aziz, *Chem. Soc. Rev.*, 2019, **48**, 558–636.
27 Y. He, Y. R. Huang, Y. L. Li, H. H. Li, Z. R. Chen and R. Jiang, *Inorg. Chem.*, 2019, **58**, 13862–13880.
28 H. Lian, X. Cheng, H. Hao, J. Han, M. Lau, Z. Li, Z. Zhou, Q. Dong and W. Wong, *Chem. Soc. Rev.*, 2022, **51**, 1926–1982.
29 W. Wu, X. L. Lin, Q. Liu, Y. He, Y. R. Huang, B. Chen, H. H. Li and Z. R. Chen, *Inorg. Chem. Front.*, 2020, **7**, 1451–1466.
30 B. Chen, Y. R. Huang, K. Y. Song, X. L. Lin, H. H. Li and Z. R. Chen, *Chem. Mater.*, 2021, **33**, 2178–2186.
31 Y. R. Huang, X. L. Lin, B. Chen, H. D. Zheng, Z. R. Chen, H. H. Li and S. T. Zheng, *Angew. Chem., Int. Ed.*, 2021, **60**, 16911–16916.
32 B. Kandasamy, G. Ramar, L. Zhou, S. T. Han, S. Venkatesh, S. C. Cheng, Z. Xu, C. C. Ko and V. A. L. Roy, *J. Mater. Chem. C*, 2018, **6**, 1445–1450.
33 Y. Li, X. Zhu, Y. Li, M. Zhang, C. Ma, H. Li, J. Lu and Q. Zhang, *ACS Appl. Mater. Interfaces*, 2019, **11**, 40332–40338.
34 W. J. Sun, Y. Y. Zhao, J. Zhou, X. F. Cheng, J. H. He and J. M. Lu, *Chem. – Eur. J.*, 2019, **25**, 4808–4813.
35 J. H. Tang, T. G. Sun, J. Y. Shao, Z. L. Gong and Y. W. Zhong, *Chem. Commun.*, 2017, **53**, 11925–11928.
36 K. S. Karimov, Z. Ahmad, F. Touati, M. M. Tahir, M. M. Rehman and S. Z. Abbas, *Chin. Phys. B*, 2015, **24**, 116102.
37 H. Chan, S. H. Lee, C. T. Poon, M. Ng and V. W. W. Yam, *ChemNanoMat*, 2017, **3**, 164–167.
38 S. Goswami, A. J. Matula, S. P. Rath, S. Hedström, S. Saha, M. Annamalai, D. Sengupta, A. Patra, S. Ghosh, H. Jani, S. Sarkar, M. R. Motapothula, C. A. Nijhuis, J. Martin, S. Goswami, V. S. Batista and T. Venkatesan, *Nat. Mater.*, 2017, **16**, 1216–1224.
39 S. Goswami, S. P. Rath, D. Thompson, S. Hedström, M. Annamalai, R. Pramanick, B. R. Ilic, S. Sarkar, S. Hooda, C. A. Nijhuis, J. Martin, R. S. Williams, S. Goswami and T. Venkatesan, *Nat. Nanotechnol.*, 2020, **15**, 380–389.
40 N. D. Paul, U. Rana, S. Goswami, T. K. Mondal and S. Goswami, *J. Am. Chem. Soc.*, 2012, **134**, 6520–6523.
41 S. Goswami, D. Sengupta, N. D. Paul, T. K. Mondal and S. Goswami, *Chem. – Eur. J.*, 2014, **20**, 6103–6111.
42 A. K. W. Chan, M. Ng, Y. C. Wong, M. Y. Chan, W. T. Wong and V. W. W. Yam, *J. Am. Chem. Soc.*, 2017, **139**, 10750–10761.
43 Y. Li, L. Chen, Y. Ai, E. Y. H. Hong, A. K. W. Chan and V. W. W. Yam, *J. Am. Chem. Soc.*, 2017, **139**, 13858–13866.
44 P. Wang, Y. Fang, J. Jiang, Y. Ji, Y. Li, J. Zheng, Q. Xu and J. Lu, *Chem. – Asian J.*, 2017, **12**, 1790–1795.
45 E. Y. H. Hong, C. T. Poon and V. W. W. Yam, *J. Am. Chem. Soc.*, 2016, **138**, 6368–6371.
46 E. Y. H. Hong and V. W. W. Yam, *ACS Appl. Mater. Interfaces*, 2017, **9**, 2616–2624.
47 J. Fang, H. You, J. Chen, J. Lin and D. Ma, *Inorg. Chem.*, 2006, **45**, 3701–3704.
48 G. Bieker, D. Diddens, M. Kolek, O. Borodin, M. Winter, P. Bieker and K. Jalkanen, *J. Phys. Chem. C*, 2018, **122**, 21770–21783.
49 K. Hossain and A. Majumdar, *Inorg. Chem.*, 2022, **61**, 6295–6310.
50 D. S. Auld, *Biometals*, 2001, **14**, 271–313.
51 W. N. Lipscomb and N. Sträter, *Chem. Rev.*, 1996, **96**, 2375–2434.
52 Z. R. Chen, J. H. Li and H. J. Li, *Chin. J. Struct. Chem.*, 2000, **19**, 389–390.
53 Z. R. Chen, J. H. Li, H. J. Li, W. P. Su and R. Cao, *Chin. J. Struct. Chem.*, 2000, **19**, 11–14.
54 A. Müller, J. Schimanski and U. Schimanski, *Angew. Chem., Int. Ed. Engl.*, 1984, **23**, 159–160.

55 A. K. Verma, T. B. Rauchfuss and S. R. Wilson, *Inorg. Chem.*, 1995, **34**, 3072–3078.
56 J. Han, H. Lian, X. Cheng, Q. Dong, Y. Qu and W. Y. Wong, *Adv. Electron. Mater.*, 2021, **7**, 2001097.
57 H. Tian, L. F. Zhao, X. F. Wang, Y. W. Yeh, N. Yao, B. P. Rand and T. L. Ren, *ACS Nano*, 2017, **11**, 12247–12256.
58 K. Song, H. Yang, B. Chen, X. Lin, Y. Liu, Y. Liu, H. Li, S. Zheng and Z. Chen, *Appl. Surf. Sci.*, 2023, **608**, 155161.
59 H. Li, Q. Xu, N. Li, R. Sun, J. Ge, J. Lu, H. Gu and F. Yan, *J. Am. Chem. Soc.*, 2010, **132**, 5542–5543.
60 Q. F. Gu, J. H. He, D. Y. Chen, H. L. Dong, Y. Y. Li, H. Li, Q. F. Xu and J. M. Lu, *Adv. Mater.*, 2015, **27**, 5968–5973.
61 Y. Y. Zhao, W. J. Sun, J. H. He and J. M. Lu, *Adv. Electron. Mater.*, 2019, **5**, 1800964.
62 Y. He, G. Ma, X. Zhou, H. Cai, C. Liu, J. Zhang and H. Wang, *Org. Electron.*, 2019, **68**, 230–235.
63 E. Cho, S. M. Pratik, J. Pyun, V. Coropceanu and J. L. Brédas, *ACS Mater. Lett.*, 2022, **4**, 2362–2367.
64 S. R. Zhang, L. Zhou, J. Y. Mao, Y. Ren, J. Q. Yang, G. H. Yang, X. Zhu, S. T. Han, V. A. L. Roy and Y. Zhou, *Adv. Mater. Technol.*, 2019, **4**, 1800342.
65 S. Chadwell, D. Rickard and G. Luther, *Electroanal.*, 2001, **13**, 21–29.
66 K. M. Schaich and C. A. Rebello, *Cereal Chem.*, 1999, **76**, 748–755.